Design of a novel magnetorheological damper with internal pressure control

Nicola Golinelli, Andrea Spaggiari
Department of Sciences and Methods for Engineering
University of Modena and Reggio Emilia, Italy
nicola.golinelli@unimore.it, andrea.spaggiari@unimore.it

ABSTRACT. In this work we designed and manufactured a novel magnetorheological (MR) fluid damper with internal pressure control. Previous authors' works showed that the yield stress τB of MR fluids depends both on the magnetic field intensity and on the working pressure. Since the increase of the magnetic field intensity is limited by considerations like power consumption and magnetic saturation, an active pressure control leads to a simple and efficient enhancement of the performances of these systems. There are three main design topics covered in this paper about the MR damper design. First, the design of the magnetic circuit; second the design of the hydraulic system and third the development of an innovative pressure control apparatus. The design approach adopted is mainly analytical and provides the equations needed for system design, taking into account the desired force and stroke as well as the maximum external dimensions.

KEYWORDS. Magnetorheological damper; Design and manufacturing; Squeeze-strengthen effect.

INTRODUCTION

Nowadays, there are several industrial applications in which magnetorheological fluids (MRFs) are used [1-3]. In particular, this paper focuses on the optimal design methodology for magnetorheological dampers (MRDs). The purpose of traditional dampers, or so-called shock absorbers, is to dissipate energy. MRDs compared to traditional dampers, exploit the change in the rheological behavior of MR fluids in order to achieve variable damping properties. The changing of the properties of MR fluids occurs when a magnetic field is applied. The magnetic field is typically generated by an axial coil, for which connecting leads are usually brought out through the hollow piston rod [4]. The main classification for MRDs concerns the methods by which the insertion volume of the rod is accommodated. This is a major design problem because the oil itself is nowhere near compressible enough to accept the internal volume reduction of 10% or more associated with the full stroke insertion. The aim of this work consists in exploiting the effect of pressure on MRFs to generate further controllable damping force, so accommodating the change in volume is very important. Clearly, a static pressure can be applied only when nearly incompressible material are used in the system, so no air or gases are allowed in the design. Several studies have been carried out in order to comprehend the influence of pressure on the properties of MRFs. In [5], a novel compressible MR fluid has been synthesized with additives that provide compressibility to the fluid. MR fluids are influenced by the presence of internal pressure [6-11]. In combined squeeze-shear mode, with a magnetic field of 300 mT, passing from 0 to 30 bar the yield shear stress to doubles its value. In flow mode instead, with a magnetic field intensity of 800 mT, the yield stress τ_B increments its value by nearly ten times. There are three basic MRDs architectures [4], as is shown in Fig. 1: single-tube, double-tube and through-rod.
The single-tube architecture (Fig. 1a) is based on a single-rod cylinder structure, in which the piston head divides the damper into extension and compression chamber. During piston movement, MR fluid passes through the control valve which is obtained into the piston head. A floating piston separates the MRF from the accumulator filled with compressed

gas. The accumulator is used to compensate the volume change due to the piston rod moving inward the cylinder. To eliminate the floating piston, emulsified oil may be used, distributing the expansion and rod-accommodation volume throughout the main oil volume. The gas separates, but quickly re-emulsifies on action. The valves must be rated to allow for the passage of emulsion rather than liquid oil. Mineral damper oil has long chain hydrocarbon molecules which do not pack efficiently together. This allows a higher compressibility than a liquid such as water because the long molecular chains can distort. In the double-tube type of telescopic (Fig. 1b), a pair of concentric cylinder is used. The external one contains some gas to accommodate the rod displacement volume. The through-rod telescopic (Fig. 1c) avoids the displacement volume issue by having a passing-through rod which causes no volume variation. However this has several disadvantages; there are external seals at both ends subject to high pressures that causes additional friction, the protruding free end may be inconvenient or dangerous, and there is still no provision for thermal expansion of the oil. However it is a simple solution which is used for example in some seismic application. Even though this architecture has proved impractical for suspension damping, it is sometimes used for damping of the steering.

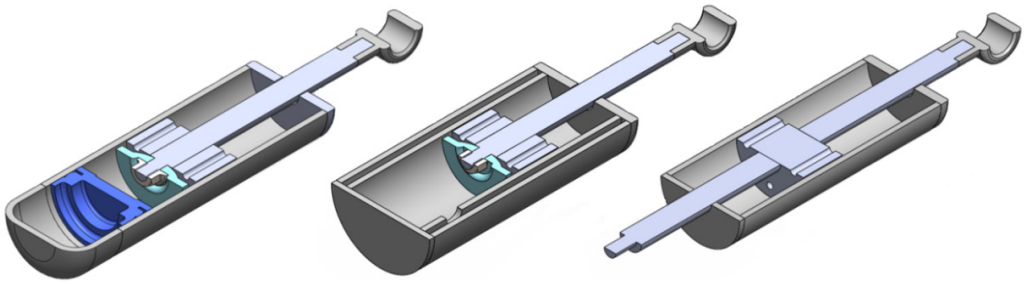

(a) (b) (c)

Figure 1: Telescopic architectures. Single-tube (a), double-tube (b) and through-rod (c).

MATERIALS AND METHODS

Since the active control of the pressure is needed, no flexible diaphragms or compressible gases are allowed. This is because flexible parts would absorb the change in pressure. Hence, it is necessary an architecture without volume compensation. Fig. 2 shows the conceptual scheme of the damper presented in this paper. We used a bottom-rod fixed to the end plug and coupled with the piston head. The bottom-rod has the same diameter of the upper-rod so that there is no volume variation. During piston movement, the bottom-rod is moving inward the chamber obtained into the piston head. The chamber is also directly connected to the canal through the upper-rod in order to bring out the coil's wire. Thereby, overpressure or depression within the chamber will not occur. It is worth noting that two coils were adopted. In this way, the longer axial length of the piston head is exploited to maximize the concatenated magnetic flux. The main dimensions of the damper are shown in Tab. 1.

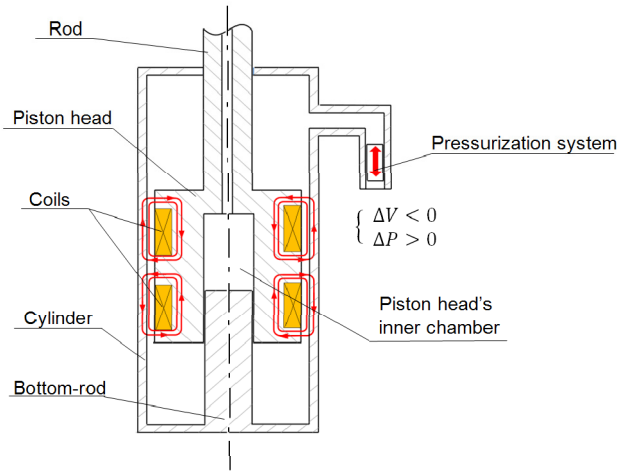

Figure 2: Conceptual scheme of the MR damper.

Cylinder length, (mm)	192
Cylinder diameter, (mm)	50
Rod diameter, (mm)	20

Table 1: Main system dimensions.

The design of the MR damper consisted in two main parts: the hydraulic-mechanical design [12, 13] and the magnetic circuit design. The specifications of the damper we developed are listed in Tab. 2.

Maximum force, (N)	2000
Maximum cylinder diameter, (mm)	40
Maximum working current, (A)	2
Maximum pressure, (bar)	40
Stroke, (mm)	50
Maximum velocity, (mm/s)	100

Table 2: Damper specifications.

In order to keep the manufacturing of the damper as simple as possible, a commercial hydraulic cylinder and the associated cylinder head were chosen [14]. Hence, knowing the outer diameter of the cylinder (50 mm) and the wall thickness (5 mm), even the inner diameter of the cylinder was also fixed (40 mm) (Fig. 3c, d). The axial length of the hydraulic cylinder is 192 mm. The commercial cylinder head is arranged for a piston rod diameter of 20 mm (Fig. 3a) and it has its own system of seals (Fig. 3b). The minimum axial length of the piston head was also fixed and had to be at least L = 90 mm. That is because we decided to compensate for the piston volume using the piston head, so it has to host a compensating bottom rod (50 mm), as presented in Fig. 2.

(a) (b) (c) (d)

Figure 3: Commercial components. Cylinder head (a) and sealing system (b). Commercial hydraulic cylinder (c) with welded boss. Bottom part of the cylinder (d).

Optimal design of magnetorheological devices requires the knowledge and the characterization of the properties of the materials involved. Firstly, the knowledge of the yield shear stress of the fluid as function of the magnetic field is necessary. The yield stress $\tau_B(\mathrm{H_{mrf}})$ of MRF 140-CG [15] is given by the experimentally-derived equation from [16, 17] and depends on the magnetic field intensity and the particle volume fraction φ:

$$\tau_B\left(H_{mrf}\right) = 271700 C \varphi^{1.5239} \tanh(6.33\times10^{-6} H_{mrf}) \quad (1)$$

φ is 0.4 and C is a coefficient dependent on the carrier fluid of the MR fluid (C = 1 for hydrocarbons), according to [17] The magnetic B-H relationship of a MR fluid can be defined as [18]:

$$B = 1.91\varphi^{1.133}\left\{1-\left[\mu_0 e^{-10.97\mu_0 H_{mrf}}\right]\right\}+\mu_0 H_{mrf} \tag{2}$$

Therefore, a MR fluid's relative permeability can be defined as:

$$\mu_r = \frac{dB}{dH_{mrf}} = 1.91\varphi^{1.133}\left(10.97\mu_0 e^{-10.97\mu_0 H_{mrf}}\right)+\mu_0 \tag{3}$$

where, B is in Tesla, H_{mrf} is in A/m, and $\mu_0 = 1.25\text{x}10^{-6}$ H/m is the permeability of free space. Fig. 4 shows the graphs of the B-H relationship of the MRF 140-CG, the values of yield stress τ_B and the relative magnetic permeability as a function of the magnetic field intensity H_{mrf}. In order to reach the best performances, the material which composes the magnetic circuit should have high magnetic permeability and high magnetic saturation. A material with such properties is the AISI 1010, which is a low-carbon steel (C% < 0.10). This material though, is hardly available because of is being used for niche applications. Hence the AISI 430 was used. AISI 430 is a ferritic stainless steel with a high relative magnetic permeability, of about 600.

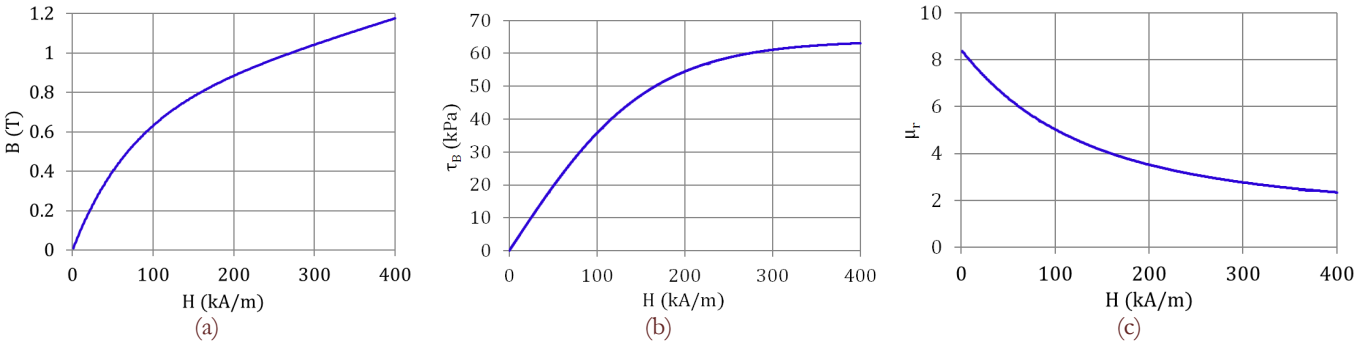

Figure 4: MRF 140 CG [15] properties: B-H relationship (a), yield stress τ_B vs H (b) and relative permeability vs H (c).

Analytical design of the MR damper

Fig. 5 shows the forces developed by a magnetorheological damper [19, 20]. Considering the parallel-plate Bingham model, the forces can be decomposed into three contributions [21]. First, the controllable force F_τ, Eq. (4), directly correlates with the magnetic field applied through the yield stress τ_B.

$$F_\tau = c\frac{\tau_B L_P A_A}{h} sign(V_D) \tag{4}$$

where L_P is the axial activation length of the piston head, A_A is the annular piston's area, h is the fluid gap and c is a coefficient that depends on the volumetric flow rate, the viscosity and the yield stress. Second, F_η, Eq. (5), represents the viscous forces and depends on the length of the orifice, the fluid's viscosity and flow rate.

$$F_\eta = k\frac{12\eta Q L A_A}{wh^3} \tag{5}$$

where Q is the flow rate, L is the total axial length of the piston head, w is the mean circumference of the damper's annular flow path and k is a constant depending on the volumetric flow rate and the velocity. Third, F_f that stands for the friction forces like those related to the seals system. Moreover we should also account for the force derived from the effect of pressure F_P. Hence, the total force will be obtained by adding up all these contributions:

$$F_{tot} = F_\tau + F_\eta + F_f + F_P \tag{6}$$

The Dynamic Range D, is also a fundamental parameter which provides an estimate of the influence of the control variable on the system behavior. D can be calculated as the controllable forces divided by the uncontrollable forces (Eq. 7).

$$D = \frac{F_c}{F_{un}} = \frac{F_\tau + F_\eta + F_f}{F_\eta + F_f} \tag{7}$$

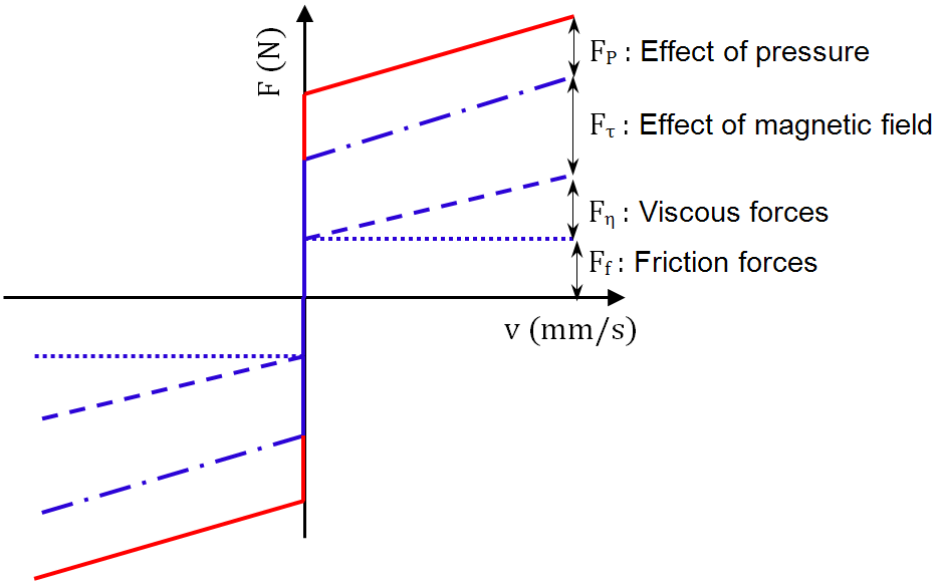

Figure 5: The total force of MRDs can be obtained by summing: friction (dotted blue line), viscous (dashed blue line), magnetic (dash-dotted blue line) and pressure (solid red line) driven forces.

Eq. (4)-(7) were manipulated taking into account the geometrical constraints and the design parameter of the remaining components were determined. In particular, considering that a fluid gap h=1 mm was chosen, the annular area A_A is 819.24 mm^2 and the viscous forces can be calculated as follow:

$$F_\eta = \left(1 + \frac{wbV_D}{2Q}\right)\frac{12\eta QLA_A}{wb^3} = \left(1 + \frac{122.26 \cdot 1 \cdot 100}{2 \cdot 81954}\right)\frac{12 \cdot 3 \times 10^{-7} \cdot 81954 \cdot 90 \cdot 819.24}{122.26 \cdot 1^3} = 191N \tag{8}$$

In which the velocity V_D=100 mm/s and the viscosity η=0.3 Pa·s. Assuming that the friction forces F_f = 250 N and the total force F_{tot} = 2000 N, the required controllable force F_τ is:

$$F_\tau = 2000 - \left(F_\eta + F_f\right) = 2000 - \left(191 + 250\right) = 1559\,N \tag{9}$$

and the dynamic range turns out to be:

$$D = \frac{F_\tau + F_\eta + F_f}{F_\eta + F_f} = \frac{1559 + 191 + 250}{191 + 250} = 4.53 \tag{10}$$

Once the controllable force was found, the yield stress of the fluid τ_B = 20 kPa was set, considering the nominal working current value I = 1 A. The total active pole length is obtainable by manipulating Eq.(4):

$$L_{P_{tot}} = \frac{F_\tau h}{c\tau_B A_A} = \frac{1559 \cdot 1}{2.30 \cdot 0.020 \cdot 819.24} = 41.32\,\text{mm} \tag{11}$$

where the coefficient c = 2.30 [12]. The activation areas are four, which implies a single axial length $L_P = L_{P_{tot}} / 4 \cong 10\,\text{mm}$. The chosen yield stress implies, by means of the Eq. (1)-(2), a magnetic field density B_{mrf} along the active pole of 0.35 T. After that, the piston head (Fig. 6a) along with the flange (Fig. 6b, c), the rod (Fig. 6d) and the bottom-rod (Fig. 6e) were manufactured. The piston head and the flange were made of AISI 430. Conversely, the rod and the bottom-rod were made of brass because they do not have to influence the magnetic flux during operations. The flange is coupled with the rod by a drilled screw in order to let the coil's wire passing through it (Fig. 6f).

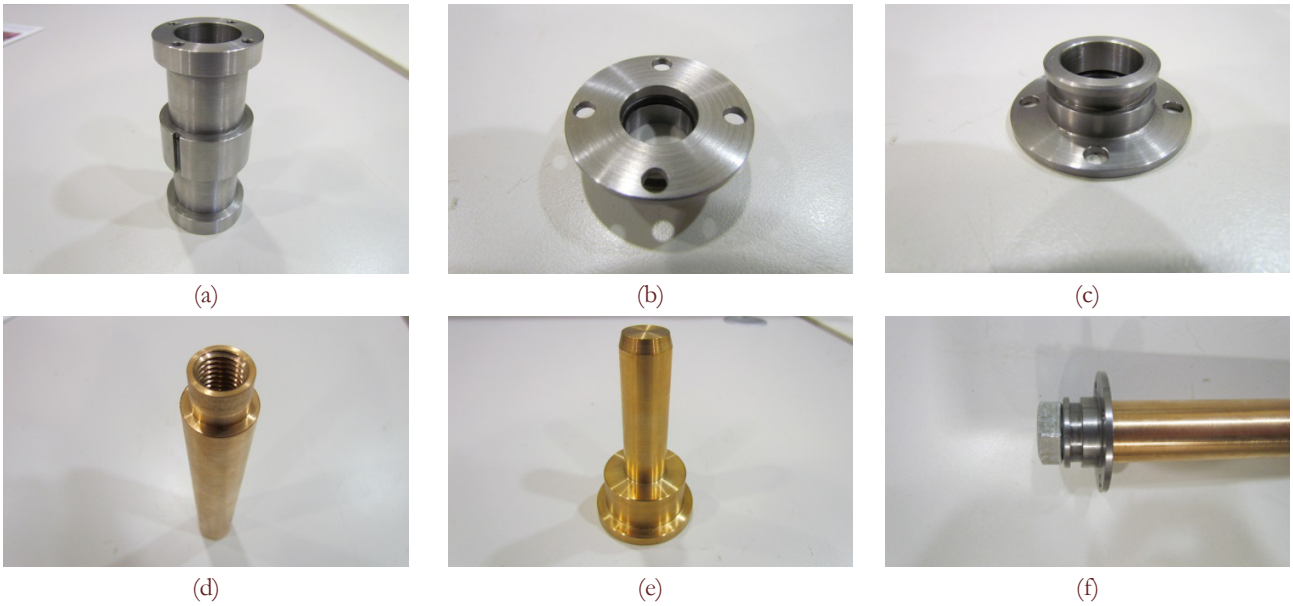

Figure 6: Custom components. Piston head (a), flange (b, c), rod (d) and bottom-rod with end plug (e). Coupling between rod and flange (f).

Design of the magnetic circuit

The aim in the design of a magnetic circuit is to determine the necessary amp-turn (NI) able to develop the required magnetic field and therefore the required damping forces. An optimal design requires to reach the desired magnetic field induction in the fluid gap while minimize the energy lost in steel flux conduit and region of non-working area. The entire circuit should have low reluctance, so soft iron or high permeability steel should be used. For an MR liquid, the permeability may be quite low, as shown in Fig. 4c. At high flux density, the iron may saturate, and be a limiting factor, so the cross-section of the iron must be adequate all around the magnetic circuit. The total flux in the circuit is the same at all sections around the circuit, so the critical point of the iron is the part with the lower cross-sectional area. The number of coils may vary to meet system requirements. Fig. 7a shows the most common configuration in which the flux lines flow around a single coil. The last two configurations in Fig. 7 have multiple coils and similar characteristics, except for the polarity of the magnetic field. In configuration Fig. 7b, the magnetic flux lines have all one only direction from the center of the solenoid. In configuration Fig. 7c, there is a trade-off between the different coils, which also affects the circuit length. The main advantage of this solution is a decrease of the overall inductance of the circuit that allows, compared to other, less response time of the same device.

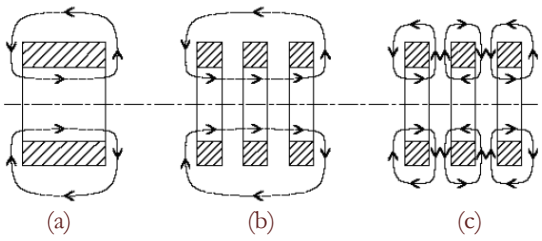

Figure 7: Coil configurations. Single coil (a), coherent multiple coils (b), incoherent multiple coils (c).

The typical design process for a magnetic circuit can be summarized as follow [14]:

- Determine the magnetic induction B_{mrf} in the MR fluid to give the desired yield stress τ_B.
- Determine the magnetic field intensity H_{mrf} by using the B-H relationship of the fluid.
- The magnetic induction flux is given by $\phi = B_{mrf} A_{mrf}$, in which A_{mrf} is the effective area of activation of the fluid. Since the magnetic induction flux remains constant through all the circuit length, calculate the magnetic induction in the steel B_{steel}:

$$B_{steel} = \frac{\phi}{A_{steel}} = \frac{B_{mrf} A_{mrf}}{A_{steel}} \tag{12}$$

– Determine the magnetic field induction B_{steel} using its B-H relationship.
– Find the required number of amp-turns (NI) by using Kirchhoff's Law of magnetic circuits:

$$NI = \sum H_i L_i = H_{mrf} h + H_{steel} L \tag{13}$$

where h is the fluid gap and L is the single length of each links which compose the circuit. The required number of coil wire resulted N = 160, considering a working current of 1 A.

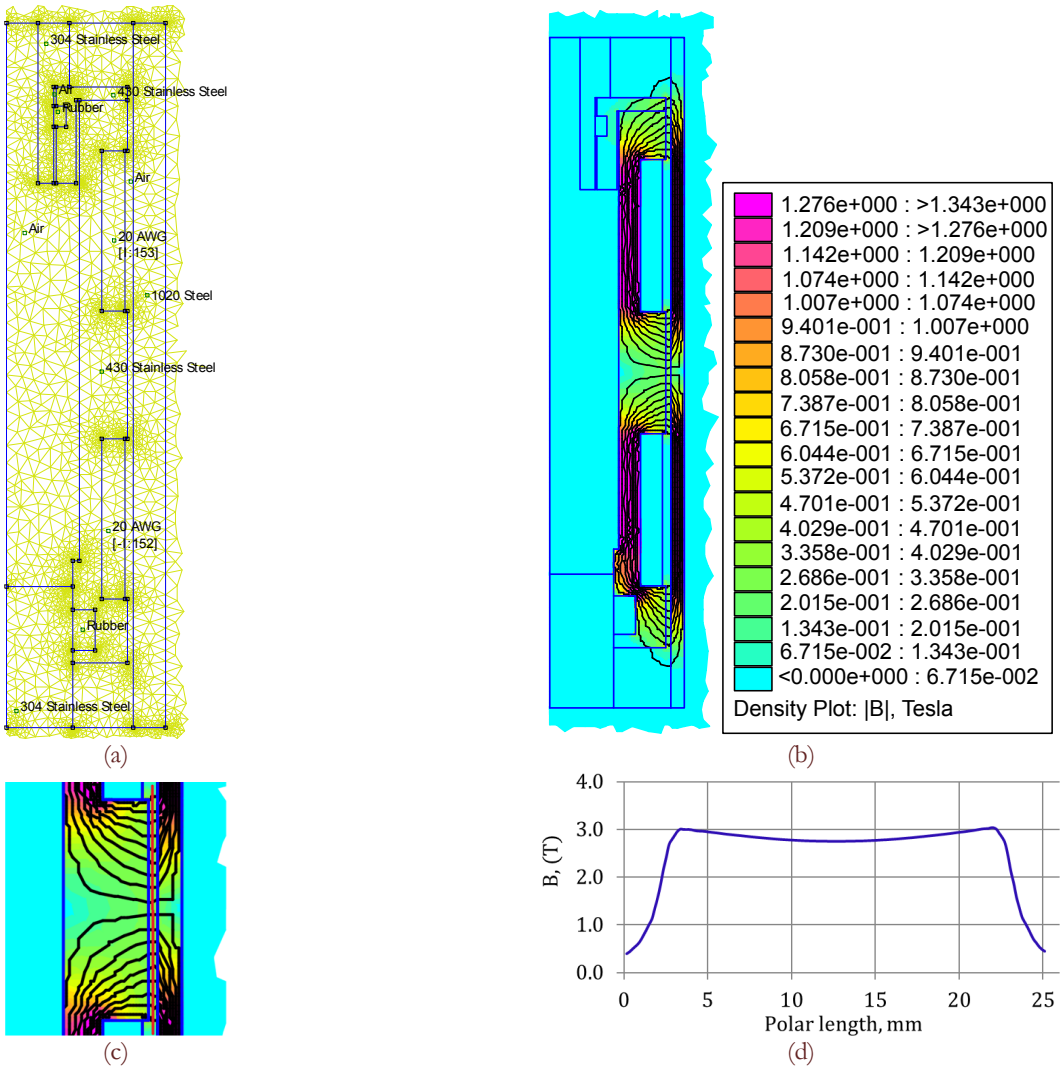

Figure 8: 2D FEMM Model of the piston head (a), magnetic field values through the magnetic circuit (b). Magnification of the central activation area (c) and graph of the magnetic field values B across the activation's gap along the red line (d).

MAGNETIC FINITE ELEMENT ANALYSIS

A magnetic finite element analysis was performed after the analytical design of the circuit. This operation is a useful method to compare the calculated values with the simulated ones. Furthermore, these simulations allow one to verify that the magnetic saturation will occur in no section of the magnetic circuit. The software FEMM v4.2 [22]

was adopted to perform all the simulations. Fig. 8a represents the discretized axially-symmetric model of the magnetic circuit which comprehends part of the piston head, the flange and the cylinder's wall. The material chosen came from the FEMM material library. AISI 430 was used for the piston head and the flange. Since the material of the hydraulic cylinder is not clearly identified by the producer, a plausible material in terms of magnetic properties was used, which is AISI 1020. For the MR fluids, a new material was set up with the magnetic properties described by Eq. (2). Fig. 8b shows the path of the magnetic flux and the values of the magnetic field density resulted whit a working current of 1 A. As it can be seen the values of B are lower than 1.5 T that is a critical point after which begins saturation. At the beginning of the design, considering the damping force required and a current of 1 A, a yield stress τ_B = 20 kPa was needed. That implied a magnetic field of B_{mrf} = 350 mT along the activation area. Fig. 8c represents a magnification of the central activation area along with the magnetic flux lines and in Fig. 8d the relative values of magnetic field. The simulated values of magnetic field density are slightly lower than those desired. A possible explanation is that the magnetic properties of the AISI 1020 do not match exactly those of the original material, which is Fe 510.

PRESSURIZATION SYSTEM

The aim of the pressurization system is the active regulation of the fluid pressure. This task has to be done in a totally controllable manner without the aid of volumetric pumps, which are incompatible with MR fluids because of the too high viscosity. Moreover, in hydraulic centralized circuits that use volumetric pumps the pressure regulation is quite expensive in terms of energy required because both the circuit and the control unit have to be constantly working in order to maintain the desired pressure. Contrarily, the new system presented does not need a continuous supply of electrical power. The designed pressurization system is schematically shown in Fig. 9.

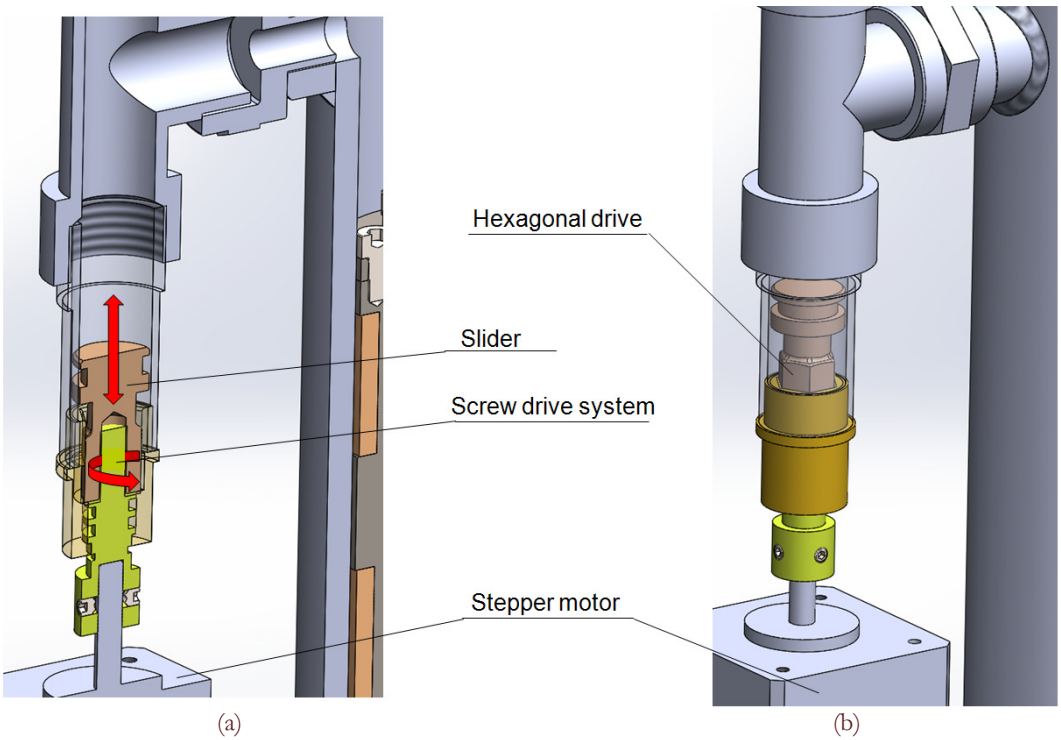

Figure 9: Pressurization system. Low pressure configuration (a) and high pressure configuration (b).

The system is composed of a stepper motor that converts the motion from rotary to translatory by a screw and nut mechanism. This system controls a slider that insists on the volume of MR fluid. Lowering the volume of fluid causes an increase of the internal pressure. Such system would be energetically convenient compared with other linear actuators currently present on market, for example coil valves. Indeed, due to the friction forces between the threads there is no retrograde motion. Hence, the desired static pressure level can be maintained with no power consumption. The MR fluid

used is a silicone-based fluid that is quite compressible (bulk modulus β of about 1000 MPa) so a pressure control not excessively abrupt is allowed.
Considering the low compressibility of the fluid, varying the value of pressure requires slider's strokes of few millimeters. The stroke of the slider is calculated analytically knowing the bulk modulus β, the total volume of the fluid V and the desired pressure variation. The equations involved are:

$$\beta = -\frac{\Delta P}{\Delta V} V \tag{14}$$

$$\Delta V = -\frac{V}{\beta} \Delta P \tag{15}$$

$$\Delta x = \frac{\Delta V}{A_{cu}} \tag{16}$$

By combining Eq. (15)-(16):

$$\Delta x = \frac{V}{A_{cu} \beta} \Delta P \tag{17}$$

In which A_{cu} is the area of the slider. Stepper motors are the most suitable for this application. By knowing the number of steps and the screw pitch an accurate control of the slider's stroke Δx is possible without position sensor.

RESULTS AND DISCUSSIONS

Fig. 10 shows the section of the 3D model of the damper. To allow the assembly, the piston head is composed of two parts: the main body of the piston head and the flange. The flange connects the piston head to the upper-rod using four screws M4x6. Particular attention was paid for the sealing system. A dynamic rod seal was used between the bottom part of the piston head and the bottom rod. Moreover, two static seal (O-Ring) were adopted between the flange and the inner chamber of the piston head. As it can be seen in Fig. 11, the coil wires pass through the drilled screw, the flange and the rod.

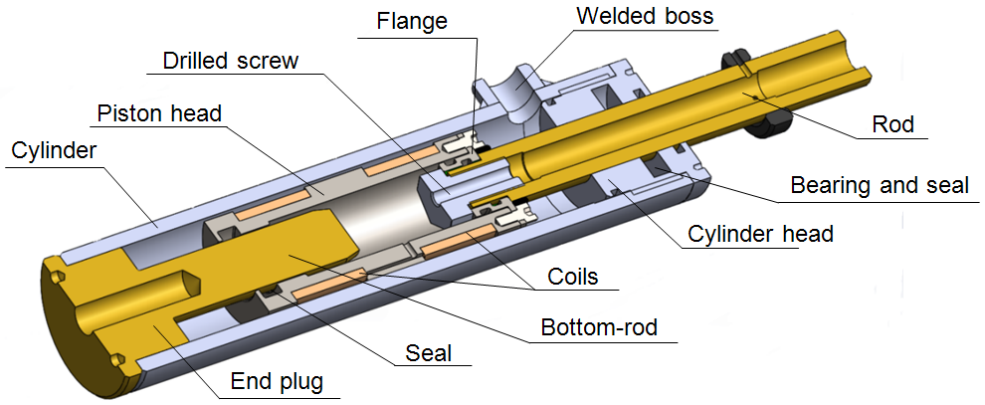

Figure 10: Cross-sectional view of the prototype of the damper.

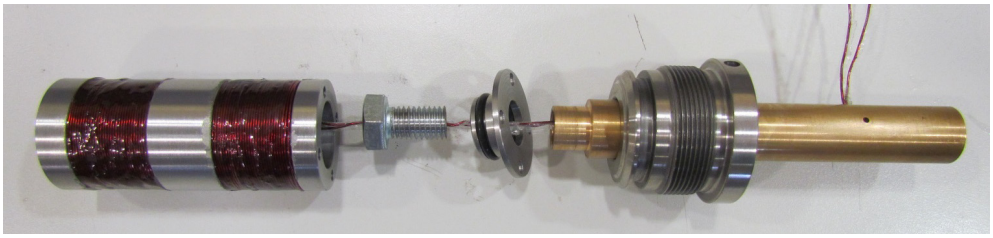

Figure 11: Exploded view. (From the right) Piston head, drilled screw, flange, rod and cylinder head.

The end-plug and the bottom-rod were glued to the cylinder using an acrylic adhesive (LOCTITE 638). The MR fluid was poured through the welded boss into the cylinder. To eliminate the air into the damper, the system was placed in a vacuum chamber. Then, two ball joint ends were screwed to the rod and the end plug (Fig. 12).

Figure 12: Final assembled prototype.

CONCLUSION

This work shows a design method for a magnetorheological damper with pressure control. By means of analytical equations the magnetic circuit and the hydraulic circuit have been designed. The new MR damper has an innovative architecture able to drive the internal pressure level. A bottom-rod has been adopted which has the same diameter of the upper rod. The main consequence is that the internal volume of the damper remains constant during the operation and an accumulator is no more needed. In order to increase the feasibility of the prototype, commercial components were used: a hydraulic cylinder, its cylinder head and two ball joint ends. Instead, the piston rod, the piston head and the bottom rod were designed and manufactured. Finally, all components were assembled paying particular attention to the concentricity between the cylinder, the piston head and the bottom rod. A conceptual design of pressurization system has also been presented. Such system consists of a screw drive mechanism that controls the stroke of a slider. Moving the slider leads to control the internal volume of the damper and consequently changes the internal pressure. To our best knowledge the prototype presented is the first of its kind ever realized. Several tests will be carried out to test the behavior of this device. The results might bring up new considerations that could lead to an optimization of the properties of the damper and to its commercialization.

BIBLIOGRAPHY

[1] Kaluvan, S., Choi, S.-B., Design of current sensor using a magnetorheological fluid in shear mode, Smart Mater. Struct., 23(12) (2014) 127003.
[2] Alkan, M. S., Gurocak, H., Gonenc, B., Linear magnetorheological brake with serpentine flux path as a high force and low off-state friction actuator for haptics, J. Intell. Mater. Syst. Struct., 24(14) (2013) 1699–1713.
[3] Yadmellat, P., Kermani, M. R., Adaptive modeling of a magnetorheological clutch, IEEE/ASME Trans. Mechatronics, 19(5) (2014) 1716–1723.
[4] Zhu, X., Jing, X., Cheng, L., Magnetorheological fluid dampers: A review on structure design and analysis, J. Intell. Mater. Syst. Struct., 23(8) (2012) 839–873.
[5] Fuchs, A., Rashid, A., Liu, Y., Kavlicoglu, B., Sahin, H., Gordaninejad, F., Compressible magnetorheological fluids, J. Appl. Polym. Sci., 115(6) (2010) 3348–3356.
[6] Spaggiari, A., Dragoni, E., Effect of internal pressure on flow properties of magnetorheological fluids, in: ASME 2011 Conference on Smart Materials, Adaptive Structures and Intelligent Systems, 1 (2011) 7–15.
[7] Spaggiari, A., Dragoni, E., Effect of pressure on the physical properties of magnetorheological fluids, Fract. Struct. Integr., 23 (2012) 75–86.
[8] Spaggiari, A., Dragoni, E., Combined squeeze-shear properties of magnetorheological fluids: effect of pressure, J. Intell. Mater. Syst. Struct., 25(9) (2013) 1041–1053.

[9] Becnel, A. C., Wereley, N. M., Demonstration of combined shear and squeeze strengthening modes in a searle-type magnetorheometer, in: Development and Characterization of Multifunctional Materials; Modeling, Simulation and Control of Adaptive Systems; Integrated System Design and Implementation, 1 (2013) V001T03A036.
[10] Tang, X., Zhang, X., Tao, R., Rong, Y., Structure-enhanced yield stress of magnetorheological fluids, J. Appl. Phys., 87(5) (2000) 2634.
[11] Guo, C., Gong, X., Xuan, S., Qin, L., Yan, Q., Compression behaviors of magnetorheological fluids under nonuniform magnetic field, Rheol. Acta, 52(2) (2013) 165–176.
[12] Nguyen, Q., Choi, S., Optimal Design methodology of magnetorheological fluid based mechanisms, Smart Actuation Sens. Syst., (2012).
[13] Nguyen, Q.-H., Choi, S.-B., Optimal design of a vehicle magnetorheological damper considering the damping force and dynamic range, Smart Mater. Struct., 18(1) 2009) 015013.
[14] Gavin, H., Hoagg, J., Dobossy, M., Optimal design of MRF dampers, in: U.S. - Japan Workshop on Smart Structures for Improved Seismic Performance in Urban Regions, (2001) 225–236.
[15] L. Corporation, MRF-140CG Magneto-Rheological Fluid. http://www.lord.com/products-and-solutions/magneto-rheological-(mr)/product.xml/1646. (2014)-
[16] Carlson, J. D., Magnetorheological fluids, in Smart Materials, New York, NY, USA: CRC Press, (2008).
[17] Lee, J.-H., Han, C., Ahn, D., Lee, J. K., Park, S.-H., Park, S., Design and performance evaluation of a rotary magnetorheological damper for unmanned vehicle suspension systems, Scientific World Journal., (2013) 894016.
[18] Wereley, N. M., Magnetorheology: advances and applications. Royal Society of Chemistry, (2013).
[19] Jang, K.-I., Min, B.-K., Seok, J., A behavior model of a magnetorheological fluid in direct shear mode, J. Magn. Magn. Mater., 323(10) (2011) 1324–1329.
[20] Yang, G., Large-scale magnetorheological fluid damper for vibration mitigation: modeling, testing and control, University of Notre Dame, (2001).
[21] Yang, G., Spencer, B. F., Carlson, J. D., Sain, M. K., Large-scale MR fluid dampers: modeling and dynamic performance considerations, Eng. Struct., 24(3) (2002) 309–323.
[22] Meeker, D., FEMM 4.2 - Finite Element Method Magnetics Homepage. http://www.femm.info/wiki/HomePage, (2015).